Multiobjective genetic approach for optimal control of photoinduced processes

Bonacina, Luigi; Extermann, Jérôme; Rondi, Ariana; Boutou, Véronique; Wolf, Jean-Pierre

Multiobjective genetic approach for optimal control of photoinduced processes

Luigi Bonacina,[1] Jérôme Extermann,[1] Ariana Rondi,[1] Véronique Boutou,[2] and Jean-Pierre Wolf[1]
[1]*Université de Genève, GAP-Biophotonics, 20 rue de l'Ecole de Médecine, 1211 Geneva 4, Switzerland*
[2]*Université Lyon 1, CNRS, LASIM UMR 5579, bt. A. Kastler, 43 Bvd du 11 novembre 1918, F-69622 Villeurbanne, France*
(Received 26 April 2007; published 14 August 2007)

We have applied a multiobjective genetic algorithm to the optimization of multiphoton-excited fluorescence. Our study shows the advantages that this approach can offer to experiments based on adaptive shaping of femtosecond pulses. The algorithm outperforms single-objective optimizations, being totally independent from the bias of user defined parameters and giving simultaneous access to a large set of feasible solutions. The global inspection of their ensemble represents a powerful support to unravel the connections between pulse spectral field features and excitation dynamics of the sample.

DOI: 10.1103/PhysRevA.76.023408 PACS number(s): 32.80.Qk, 33.80.Wz, 82.53.−k

I. INTRODUCTION

In recent years, pulse-shaping techniques have been progressively implemented for increasing the degree of control in light-matter interactions. In order to identify the optimal pulse shape to drive a given photoprocess, a common approach relies on the systematic investigation of field interferences [1–4]. Such open-loop procedures, although quite time consuming, undoubtedly present the advantage of providing clear evidence of the processes at the origin of the selectivity of the pulse and are not limited to simple atomic and molecular systems as demonstrated by their recent application to biological samples for improving selectivity in nonlinear microscopy [5,6] and biomedical imaging techniques [6–8].

In parallel, after the suggestion of Judson and Rabitz [9], closed-loop learning procedures based on genetic algorithms (GAs) have contributed to a number of successful experiments, ranging from steering of molecular reactions in gas [10,11] and condensed [12] phases to high-harmonic generation [13] and control of fundamental biophysical processes [14–16]. Despite their versatility and convergence rapidity, GA-based approaches are subjected to a series of criticisms concerning the robustness of the solution, the difficulty to identify the global maximum, and a certain dependence of the outcome on the experimental apparatus.

Indeed the goal of the optimization is often hindered or in conflict with other experimental aspects: basic processes such as the maximization of multiphoton vibronic transitions suffer from these shortcomings, as the dominant solution, likely corresponding to transform-limited excitation, prevents the retrieval of the subtle pulse features matching the target molecule dynamics [17]. To cope with this limitation, the original optimization goal is usually modified inserting *ad hoc* cost functions, meant to avoid convergence towards unsuitable or meaningless solutions. On the other hand, this procedure may entail undesirable consequences, as the relative weights adopted for the cost functions inevitably bias the algorithm evolution and may divert the system to converge to valuable solutions.

Optimal discrimination experiments [12,18,19] share similar difficulties. The optimization goal is the selective enhancement of the signal from a specific chromophore in competition with a second one, characterized by similar or overlapping absorption bands. The target objective is typically defined as the ratio between the signals simultaneously generated by the two systems. Obviously, to avoid numerical artifacts (division by zero) or convergence to solutions yielding very small signal intensities, it is compelling to add an offset (ϵ) to the denominator and include a term (α) proportional to the quantity to maximize.

Procedures based on the parametrization of the GA target have been developed also to strengthen [20] the identification of the essential features of optimal pulses and unravel their connections to the sample photodynamics [21,22]. More recently, the issue of continuity of solution hypersurfaces has been experimentally addressed with a technique based on the introduction of a scalar variable in the GA objective [23].

In the present work, we apply an optimal control algorithm capable of handling simultaneously multiple target objectives [24]. The results demonstrate that it increases the versatility and the robustness of the GA approach, avoiding the artificial limitations dictated by user-defined scalar cost-function parameters.

To evaluate the performance of this approach, we set up a benchmark experiment based on the two-photon excitation of a molecule of biological interest: flavin mononucleotide (FMN), one of the main sources of autofluorescence in living organisms [25]. A typical application of optimal dynamic discrimination [19] could, for instance, be the efficient detection of bacteria among background aerosols that exhibit similar fluorescence emission [26,27]. Given the nonlinearity of the excitation process, the maximization of the fluorescence intensity (I_{fluo}) is expected to have a trivial solution corresponding to Fourier-transformed pulses. Following Brixner *et al.*, this dominant intensity dependence can be lifted by normalizing FMN fluorescence by the second-harmonic (SHG) signal (I_{SHG}) generated by the same shaped pulse in a nonlinear crystal [17]. In the following, we discuss the results of a systematic series of optimizations that we performed using both single (two scalar parameters α and ϵ) and multiple targets, expressed, respectively, in the form $[I_{fluo}/(\epsilon+I_{SHG})+\alpha I_{fluo}]$ and $[I_{fluo}/I_{SHG};I_{fluo}]$.

TABLE I. Algorithm parameters used for all optimizations described in this work.

Population size	20
Real variables	128
Crossover probability	8×10^{-1}
Mutation probability	1×10^{-2}
Distr. index crossover	10
Distr. index mutation	20

II. METHODS

A. NSGA-II algorithm

We adapted to our experimental needs the elitist nondominated sorted GA (NSGA-II) developed by Deb *et al.* [24]. In this section, we summarize its main differences with respect to GAs typically employed for coherent control of photodynamics [28,29].

NSGA-II varies from single-objective GAs substantially in the way the selection operator acts. The key concept is associated with the notion of *domination*: a solution is said to dominate another solution if it is not worse in any of the objectives and it is strictly better in at least one. Conversely, a solution is *nondominated* if no solution can be found that dominates it. After random initialization, at the ith iteration, the population P_i of size N generates an offspring population Q_i of N new individuals by standard tournament selection, recombination, and mutation operators. The combined population $R_i=P_i\cup Q_i$ is successively sorted according to nondomination: the solutions fulfilling the definition of nondomination are ranked in the first nondominated front F_i^1. If the size of F_i^1 is smaller than N, all its members are retained in the next parent population P_{i+1}. The remaining individuals of P_{i+1} are selected in the next nondominated front F_i^2, computed after eliminating F_i^1 from R_i. The same procedure is continued until a set—say, F_i^n—cannot be entirely accommodated in P_{i+1}. The elements of F_i^n are then sorted according to the crowding distance operator, which is introduced for preserving the population diversity. The difference among the individuals is calculated in the multidimensional target space from the signals generated on each objective [24].

This naive description of the algorithm is sufficient to clarify the concept of *Pareto* optimal set, extensively used in the forthcoming discussion, which simply corresponds to the final set of nondominated solutions. The latter are assumed to balance the objectives in a unique and optimal way.

For this study we used a real codification of the NSGA-II algorithm. We restricted the optimizations to a maximum of two objectives, even if there is no computational limitation regarding this point. The parameters used for the measurements are summarized in Table I. We did not perform any systematic study of these values for improving convergence speed and/or quality of the outcome, our interest being limited to a straight comparison between single- and multiple-objective approaches.

B. Experiment

The prism compression of a Ti:sapphire oscillator, capable of delivering 15-fs pulses, was adjusted to limit the output bandwidth to 12 nm full width at half maximum (FWHM). This precaution was necessary to prevent the pulse spectrum dispersed by a 1200-grooves/mm gold grating to exceed the size of our liquid-crystal pulse shaper (SLM-256, CRI) placed at the Fourier plane of a zero-dispersion compressor in a 4-f arrangement. Simultaneous amplitude and phase modulation was performed addressing a total of 128 independent pixels on the double liquid-crystal array. Note that no calibration procedure was applied as the algorithm was addressing directly the driving voltages of the active elements as optimization variables. The shaped pulses were separated by a pellicle beam splitter ($R/T=8/92$, 2 μm thickness) into two distinct optical paths. The reflected beam, focused by a 5-cm lens onto a 150-μm-thick BBO crystal, was used to generate the SHG signal detected by a photodiode equipped with a 40-nm bandpass filter at 400 nm. The transmitted part (50 mW average power) was focused by an identical lens, onto a 1-mm suprasil flow cell where the FMN sample was constantly refreshed. The fluorescence signal was collected by two lenses, spectrally filtered by means of a BG40 Schott glass and a 40-nm bandpass filter centered at 500 nm and detected by a photomultiplier tube. Both signals were fed into two independent lock-in amplifiers, before being acquired by computer, and processed to provide feedback to the GA. For each sensitivity setting, the linearity in the response of both arms was carefully checked throughout the accessible dynamic range by measuring the signals generated by an unmodulated pulse at different intensities. Frequency-resolved optical gating (FROG) traces were systematically acquired at the end of each optimization run with a commercial SHG FROG device (Pulsecheck, APE Berlin).

The FMN solution was prepared using flavin mononucleotide from Sigma-Aldrich, dissolved in water at a concentration of 2 g/l.

III. RESULTS AND DISCUSSION

Figure 1 displays the comparison between the evolution of a single-objective optimization of $[I_{fluo}/(I_{SHG}+\epsilon)+\alpha I_{fluo}]$ [panel (a)] and that of a run of the NSGA-II algorithm simultaneously maximizing $[I_{fluo}/I_{SHG};I_{fluo}]$ [panels (b) and (c)].

In (a), we observe the monotonous growth of the discrimination ratio I_{fluo}/I_{SHG} generated by the best individual of each generation. Notice that the plotted quantity differs from the actual feedback signal. At the beginning of the optimization, we identify a transient phase of 10–20 generations characterized by $I_{fluo}/I_{SHG}<1$. This regime is associated with larger efficiency of the SHG process with pulses with random amplitudes and spectral phases. Since we carefully verified the linearity and the balance between the two optical arms, this finding does not constitute a major limitation for the optimization. After this short phase, the discrimination ratio steadily increases with values constantly above 1. After $\sim$120 generations, it converges to a final value of 1.25.

The evolution driven by the multiobjective algorithm depicted in Figs. 1(b) and 1(c) is somehow less straightforward. During the first generations, the algorithm output is associated with a single solution per iteration, evidencing the exis-

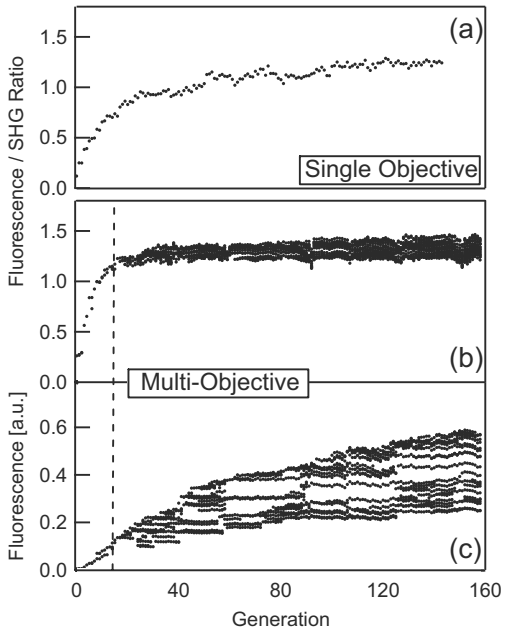

FIG. 1. Comparison between the evolution of a single-objective optimization of $[I_{fluo}/(\epsilon+I_{SHG})+\alpha I_{fluo}]$ with $\alpha=0$, $\epsilon=0.3$, and that of a run of the NSGA-II algorithm maximizing simultaneously $[I_{fluo}/I_{SHG};I_{fluo}]$. Evolution of the discrimination ratio I_{fluo}/I_{SHG} in the single-objective (a) and in the multiobjective (b) cases. (c) Evolution of I_{fluo} in the multiobjective run.

tence of an individual exhibiting simultaneously the greatest discrimination ratio and fluorescence intensity. Once the system has exited this region (dashed vertical line), the number of feasible solutions suddenly inflates, eventually saturating the number of individuals in the population $[\dim(F^1_{i>40})>N]$. This behavior is representative of conflicting targets. In fact, consistently with the nondomination ranking performed by the algorithm, each individual yielding high values on one target is bound to be weak on the other one. If this were not the case, there would be an individual dominating all the others and $\dim(F^1_i)=1$. We observe that the NSGA-II algorithm keeps on increasing both targets during the whole optimization. At each step, the feasible solutions represent the best compromise found between the two conflicting goals. The large distribution of the solutions is preserved by the crowding distance operator, which retains for the next optimization step the pulses characterized by maximal distance in the two-dimensional signal space. After 120 generations, as in the case of the single-objective optimization, the signals converge to steady values [24].

The result of the evolution can be more easily appreciated when I_{fluo} is plotted against the control variable (I_{SHG}) [17], as in Fig. 2. As both I_{fluo} and I_{SHG} are normalized with respect to the signal generated with a reference unmodulated pulse, the dashed diagonal line corresponds to the undiscriminating situation $I_{fluo}=I_{SHG}$. This condition was systematically verified at different intensities, as indicated by the experimental data points along the diagonal. The global output of the optimization is represented by the dots above this line, where $I_{fluo}>I_{SHG}$. They correspond to all the individuals tested during the optimization, while the circles highlight

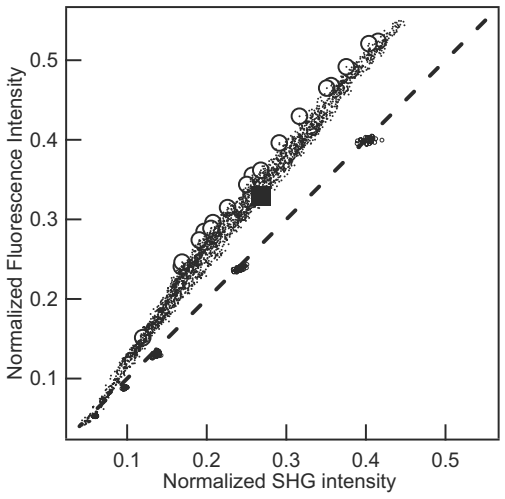

FIG. 2. Global output of the multiobjective optimization of Fig. 1. Dots: individuals tested during the evolution. Circles: final feasible population (Pareto front). Dashed line: undiscriminating solution $I_{fluo}=I_{SHG}$, retrieved by an unmodulated pulse at different intensities, as demonstrated by the experimental data points lying along the diagonal.

the final feasible population constituting the best approximation of the Pareto front of optimal solutions found by the algorithm. For comparison, the solid square indicates the final solution obtained with the single-objective optimization reported in Fig. 1(a).

The discrimination ratios of all solutions belonging to the Pareto front and their corresponding fluorescence intensities are illustrated in Fig. 3. The plot contains the results of various multiobjective (opened shapes) and single-objective (solid shapes) optimizations associated with different $[\alpha;\epsilon]$

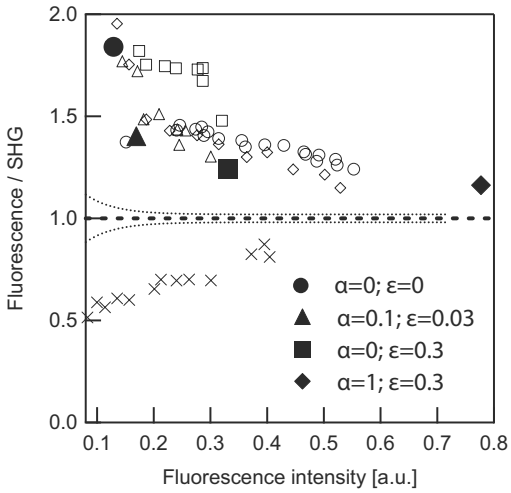

FIG. 3. Comparison between the results of several independent multiobjective (open shapes) and single-objective (solid shapes) optimizations. The single-objective GA results are obtained using different $[\alpha;\epsilon]$ parameter pairs. The crosses correspond to maximizing the opposite goal with NSGA-II, namely $[I_{SHG}/I_{fluo};I_{SHG}]$. The dotted curve indicates the experimental error at different signal intensities.

parameter pairs, together with the outcome of the optimizations presented above (solid square and open circles, respectively). The dotted line is an upper estimate of the experimental error in I_{fluo}/I_{SHG}, calculated from the dispersion of the fluorescence and SHG measurements generated by unshaped pulses at different intensities.

From this general comparison it is evident that the Pareto front is a common solution for all the optimizations and that single-target outcomes fit well in the general trend. Greater α and ϵ values give more weight to the signal intensity, leading to a solution characterized by stronger signals and weaker fluorescence and SHG discrimination. Smaller or vanishing α and ϵ values privilege the ratio at the expense of fluorescence intensity. Notice that, for all I_{fluo} values associated with solutions of the single-objective optimizations, the discrimination ratio retrieved by the multiobjective algorithm is slightly but systematically higher. It is remarkable that the same computational effort (the number of individuals tested in the various optimizations is roughly the same) gives access in the case of multiobjective optimization to a much richer ensemble of solutions without affecting, even improving, their quality. The pulse best adapted for a specific application can be readily selected within this collection.

The discriminating capacity and the signal magnitude associated to the different final pulses were tested several days after the optimization, yielding results well inside the error estimate given in the plot. As an additional check, we also performed the opposite optimization—i.e., the simultaneous maximization of $[I_{SHG}/I_{fluo};I_{SHG}]$. The crosses in Fig. 3 with ratio below unity represent the feasible solutions obtained this way. We observe a remarkable symmetry of this ensemble with respect to that obtained by maximizing the fluorescence.

This finding is consistent with the physical explanation that can be formulated after inspection of Fig. 4(a), showing a comparison between the SHG FROG traces of two pulses respectively maximizing (left) and minimizing (right) the I_{fluo}/I_{SHG} ratio and that of a reference unmodulated pulse (center). The optimizations principally act suppressing one or the other edge component of the pulse spectrum, in order to enhance or reduce the nonlinear excitation of FMN (two-photon absorption maximum at 760 nm [30]). This strategy modulates the I_{fluo}/I_{SHG} ratio, taking into consideration that the SHG process for a 150-μm crystal is insensitive to wavelength within the excitation pulse bandwidth ($<$15 nm).

As a consequence, the FROG spectral slices taken at zero time delay in Fig. 4(b) indicate an overall bandwidth reduction of $\sim$25% for both the SHG- (I_{fluo}/I_{SHG}=0.7) and fluorescence- (I_{fluo}/I_{SHG}=1.77) enhancing pulses with respect to the reference pulse. Beside this major effect on the amplitude of the spectral components, we also observe a reduction of the pulse duration for both optimal pulses with respect to the reference one.

In Fig. 4(c), we analyze the relationship between the two targets of the multiobjective optimization presented in Fig. 2 and the position of the first spectral moment[1] of the pulses belonging to the final Pareto front. One clearly recognizes

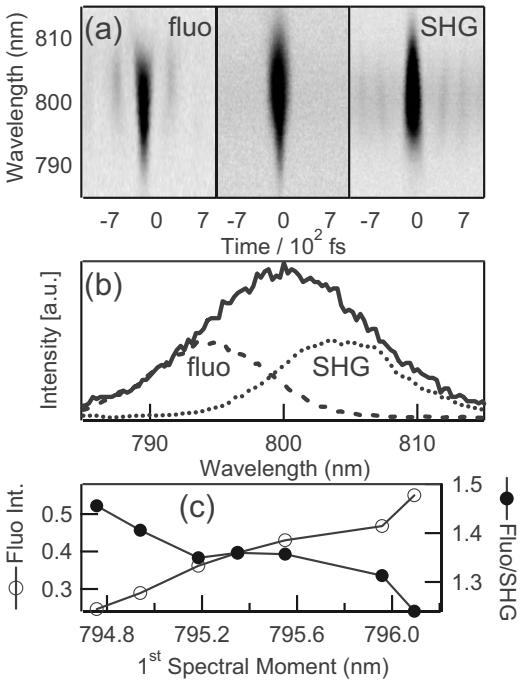

FIG. 4. (a) FROG traces corresponding to pulses maximizing FMN fluorescence (left), undiscriminating (center), and maximizing SHG (right). (b) Spectral cuts at zero time delay extracted from the FROG traces in the top panel. (c) Behavior of the multiobjective optimization targets I_{fluo} and I_{fluo}/I_{SHG} as a function of the first spectral moment of the optimal pulses retrieved by the algorithm.

the competition between the two targets: discrimination decreases as the pulse spectral edge shifts to the red, toward the laser output maximum (800 nm). At the same time, I_{fluo} increases, as the incident pulse intensity augments, enhancing nonlinear excitation. Similar trends were found for all the optimizations shown in Fig. 3, and a complementary behavior at the blue side of the spectrum was observed for the SHG maximization.

IV. CONCLUSIONS

The NSGA-II algorithm is applicable to a vast ensemble of control problems. It allows approximating the Pareto front by a large ensemble of solutions whose diversity is constantly preserved during the optimization with a computational effort comparable to traditional GAs. Picking a single solution from this set is an *a posteriori* judgement, which can be done in terms of concrete experimental needs. Moreover, we observed a slight improvement in the quality of the individual solutions retrieved by the multiobjective algorithm in comparison to the ones indicated by the single-target approach. Eliminating all scalar parameters in the objective expression (and in the crowding distance procedure [24]) assures an unbiased convergence.

The distribution of solutions in the target space gives access to primary information for unraveling the relationship between pulse spectral field features and sample photodynamics. In particular, any global trend in the final ensemble of solutions may help associating specific pulse characters to

[1]Defined as $\int I(\lambda)\lambda d\lambda / \int I(\lambda) d\lambda$.

different outcomes of the photoprocess. In this respect, the unambiguous understanding of the strategy underlying the optimizations presented in this work facilitates the comparison between the single- and multiple-objective approaches.

Finally, we observe that multiobjective optimization may improve the performances of the so-called *control pulse cleaning* procedure described by Lindinger *et al.* [31]. In that case, the optimization target is modified including a one-parameter cost function elaborated to suppress all unessential field components to facilitate the deciphering of the optimal pulse. A sensible combination of the two approaches, by introducing the genetic pressure against appearance of unnecessary pulse features as a parameter-free objective, may help to generalize the result of the optimization.

ACKNOWLEDGMENTS

This work was supported by the Swiss National Science Foundation in the framework of the CIBA (Coherent Identification of Bacteria in Air) project via Contract No. 200021-111688. We also gratefully acknowledge the support of Schmidheiny Foundation, Geneva.

[1] D. Meshulach and Y. Silberberg, Nature (London) **396**, 239 (1998).
[2] N. Dudovich, D. Oron, and Y. Silberberg, Phys. Rev. Lett. **92**, 103003 (2004).
[3] N. Dudovich, T. Polack, A. Pe'er, and Y. Silberberg, Phys. Rev. Lett. **94**, 083002 (2005).
[4] V. V. Lozovoy and M. Dantus, ChemPhysChem **6**, 1970 (2005).
[5] N. Dudovich, D. Oron, and Y. Silberberg, Nature (London) **418**, 512 (2002).
[6] I. Pastirk, J. M. Dela Cruz, K. A. Walowicz, V. V. Lozovoy, and M. Dantus, Opt. Express **11**, 1695 (2003).
[7] J. P. Ogilvie, D. Debarre, X. Solinas, J. L. Martin, E. Beaurepaire, and M. Joffre, Opt. Express **14**, 759 (2006).
[8] J. M. Dela Cruz, V. V. Lozovoy, and M. Dantus, J. Photochem. Photobiol., A **180**, 307 (2006).
[9] R. S. Judson and H. Rabitz, Phys. Rev. Lett. **68**, 1500 (1992).
[10] A. Assion, T. Baumert, M. Bergt, T. Brixner, B. Kiefer, V. Seyfried, M. Strehle, and G. Gerber, Science **282**, 919 (1998).
[11] T. Hornung, R. Meier, D. Zeidler, K. L. Kompa, D. Proch, and M. Motzkus, Appl. Phys. B: Lasers Opt. **71**, 277 (2000).
[12] T. Brixner, N. H. Damrauer, P. Niklaus, and G. Gerber, Nature (London) **414**, 57 (2001).
[13] R. Bartels, S. Backus, E. Zeek, L. Misoguti, G. Vdovin, I. P. Christov, M. M. Murnane, and H. C. Kapteyn, Nature (London) **406**, 164 (2000).
[14] V. I. Prokhorenko, A. M. Nagy, and R. J. D. Miller, J. Chem. Phys. **122**, 184502 (2005).
[15] W. Wohlleben, T. Buckup, J. L. Herek, and M. Motzkus, ChemPhysChem **6**, 850 (2005).
[16] V. I. Prokhorenko, A. M. Nagy, S. A. Waschuk, L. S. Brown, R. R. Birge, and R. J. D. Miller, Science **313**, 1257 (2006).
[17] T. Brixner, N. H. Damrauer, B. Kiefer, and G. Gerber, J. Chem. Phys. **118**, 3692 (2003).
[18] J. M. Dela Cruz, I. Pastirk, V. V. Lozovoy, K. A. Walowicz, and M. Dantus, J. Phys. Chem. A **108**, 53 (2004).
[19] B. Q. Li, H. Rabitz, and J. P. Wolf, J. Chem. Phys. **122**, 154103 (2005).
[20] A. F. Bartelt, M. Roth, M. Mehendale, and H. Rabitz, Phys. Rev. A **71**, 063806 (2005).
[21] A. Lindinger, S. M. Weber, C. Lupulescu, F. Vetter, M. Plewicki, A. Merli, L. Woste, A. F. Bartelt, and H. Rabitz, Phys. Rev. A **71**, 013419 (2005).
[22] T. Hornung, M. Motzkus, and R. de Vivie-Riedle, Phys. Rev. A **65**, 021403(R) (2002).
[23] J. Roslund, M. Roth, and H. Rabitz, Phys. Rev. A **74**, 043414 (2006).
[24] K. Deb, A. Pratap, S. Agarwal, and T. Meyarivan, IEEE Trans. Evol. Comput. **6**, 182 (2002).
[25] P. F. Heelis, Chem. Soc. Rev. **11**, 15 (1982).
[26] F. Courvoisier, V. Boutou, V. Wood, A. Bartelt, M. Roth, H. Rabitz, and J. P. Wolf, Appl. Phys. Lett. **87**, 063901 (2005).
[27] F. Courvoisier, V. Boutou, L. Guyon, M. Roth, H. Rabitz, and J. P. Wolf, J. Photochem. Photobiol., A **180**, 300 (2006).
[28] T. Baumert, T. Brixner, V. Seyfried, M. Strehle, and G. Gerber, Appl. Phys. B: Lasers Opt. **65**, 779 (1997).
[29] D. Zeidler, S. Frey, K. L. Kompa, and M. Motzkus, Phys. Rev. A **64**, 023420 (2001).
[30] G. A. Blab, P. H. M. Lommerse, L. Cognet, G. S. Harms, and T. Schmidt, Chem. Phys. Lett. **350**, 71 (2001).
[31] A. Lindinger, C. Lupulescu, F. Vetter, M. Plewicki, S. M. Weber, A. Merli, and L. Woste, J. Chem. Phys. **122**, 024312 (2005).